REAL TIME IN-SITU OBSERVATIONS OF EQUIAXED DENDRITE COHERENCY IN AL-CU ALLOYS USING HIGH BRILLIANCE 3rd GENERATION SYNCHROTRON SOURCES

Andrew G. Murphy[1], David J. Browne[1], Wajira U. Mirihanage[2], Ragnvald H. Mathiesen[2]

[1]Engineering and Materials Science Centre, University College Dublin, Ireland
[2]Deptartment of Physics, Norwegian University of Science and Technology, N-7491 Trondheim Norway

Keywords: Aluminum alloys, Dendrite coherency, Solidification, Synchrotron radiation

Abstract

In the last decade synchrotron X-ray sources have fast become the tool of choice for performing in-situ high resolution imaging during alloy solidification. This paper presents the results of an experimental campaign carried out at the European Synchrotron Radiation Facility, using a Bridgman furnace, to monitor phenomena during solidification of Al-Cu alloys - specifically the onset of equiaxed dendrite coherency. Conventional experimental methods for determining coherency involve measuring the change in viscosity or measuring the change in thermal conductivity across the solidifying melt Conflicts arise when comparing the results of these experimental techniques to find a relationship between cooling rate and coherency fraction. It has been shown that the ratio of average velocity to the average grain diameter has an inversely proportional relationship to coherency fraction. In-situ observation therefore makes it possible to measure these values directly from acquired images sequences and make comparisons with published results.

Introduction

Many casting defects, e.g. microsegregation, hot tearing, gas porosity and solidification shrinkage, develop in mush after the point of coherency is reached. Traditionally dendrite coherency has been determined by one of two methods, namely rheological [1–4] and thermal analysis [5]. Rheological methods are based on measuring the increasing viscosity of the melt, as solid becomes coherent, and ultimately the shear strength of the dendritic network. Experimental details of the rheological setup have been well described by others [6] so it will not be discussed here. Thermal analysis is based on the principle of differing thermal conductivities between solid and liquid in the solidifying melt. In both rheological and thermal experimental methods the coherency fraction solid is calculated from the thermal data and compared to various alloy and process parameters for correlation [7]. Early coherency studies compared both methods for industrial grade aluminum alloys, ultimately showing good agreement [8, 9]. Increasing either cooling rate or solute content exhibited earlier coherency and thus lower fraction solid. The addition of grain refiners decreased grain size, delaying coherency and thus increasing coherency fraction solid. Chai [6] *et al.* performed a detailed theoretical analysis, based on diffusion-controlled equiaxed growth models, predicting coherency fraction solid, which was found to depend on the competition between nucleation and growth. Typically, for alloys with solute concentrations between zero and the solubility limit, as solute concentration increases both grain size and growth rate decrease. It is, however, the faster of the two decreasing variables, i.e. grain size or growth rate, which dictates final coherency fraction solid. An inversely proportional

relationship is found for cooling rate, growth restriction faction and coherency time, the time at which the coherency-torque curve first deviates from steady state, as well as varying proportionally with *d/V*, where *d* is the grain diameter at coherency and *V* is the average dendritic growth rate. Although these theoretical predictions have been shown to underestimate the coherency fraction solid observed, they still display qualitative agreement with experimental results [9]. The most recent study of Veldman [10] *et al.* showed significant deviation between both experimental methods for Al-Si-Cu ternary alloys. In rheological experiments cooling rate was observed to have little effect on coherency fraction solid as opposed to thermal analysis which suggested the reverse. Similar results were observed when comparing solute additions with increasing silicon content observed to reduce coherency fraction solid. Silicon content is also observed to dominate, over cooling rate, the microstructure morphology, with lower levels exhibiting small globulitic structure and higher levels, larger orthogonal dendritic grains. A fullness morphological parameter, which is defined as the ratio of internal grain volume solid fraction, V_{GS}, to grain envelope volume, V_{GE}, or more traditionally the internal solid fraction, f_S, (equation (2)) [11, 12] showed high correlation with coherency fraction solid and solute additions indicating grain morphology as a controlling factor of coherency.

Many detailed solidification studies have now been conducted using binary alloy systems and synchrotron radiation and much quantitative data has been gathered and analyzed [13–15]. Following on from previous X-ray studies, this paper compares the experimental rheological and thermal coherency analysis with preliminary real time in-situ observations of equiaxed grain coherency, showing qualitative agreement with recent rheological studies.

Experimental Methods

This experimental campaign was carried out on the ID15A beamline at the European Synchrotron Radiation Facility (ESRF) in Grenoble, France. The experimental, Bridgman furnace, set up was principally the same as described in previous campaigns [16–18] and thus has been well documented. Specific parameters unique to this campaign and salient features of the rig are herein described. Two alloy sample types, Al-15wt%Cu and Al-25wt%Cu, measuring 30 x 15 x 0.2 mm, were used in this study. Grain refinement was achieved by the addition 0.5 g/kg of Al-Ti-B as described previously. Samples, once oxidized and coated with a boron-nitrite spray, are encased between two 150 μm quartz glass plates. This assembly is fitted to a translation device allowing the sample to be pulled through an imposed thermal gradient. The thermal gradient is supplied by two heater elements surrounding the crucible and separated by an adiabatic zone, where the incident X-ray beam intersects the sample. Temperature readings from the heaters are continuously measured by embedded thermocouples during the course of solidification, allowing for mid-run manual adjustment of the temperature gradient. The field of view (FOV) for captured images is set to 1.3 x 1.3 mm. Image capture was performed by a Sarnoff fast readout 512 x 512 pixel CCD, with image acquisition every 0.045 seconds. The ID15A is a high energy beamline delivering incident photons in the range [30 keV, 750 keV]. For this particular experiment the full polychromatic incident beam was employed. In terms of X-ray absorption contrast in the radiograms, however, only the lower photon energies will give a measurable contribution.

Solidification was performed by translating the sample through a constant or varying thermal gradient at a constant velocity, anti-parallel to gravity. Post experimental image enhancement and analysis is carried out using MATLAB from MathWorks, ImageJ, a java based open source image manipulation toolbox and the GNU Image Manipulation Program. Adaptive, linear and

nonlinear spatial filtering algorithms are used in conjunction with adaptive contrast enhancement and flat fielding techniques augment visible contrasts. Figure 1 shows a schematic layout of the heater/sample section of the Bridgman furnace used in the experiments. Also indicated is the location and scale of the field of view in contrast with the sample dimensions.

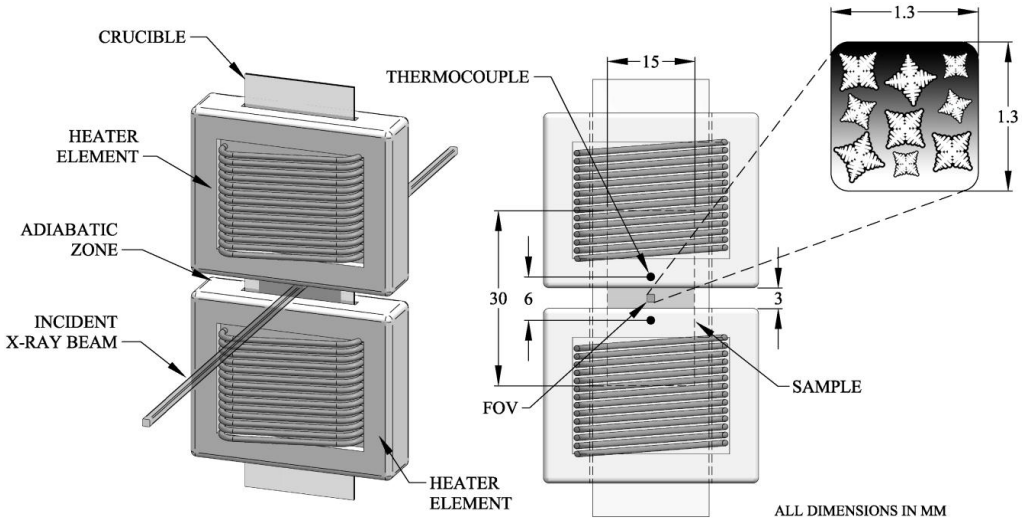

Figure 1. Schematic layout of the Bridgman type gradient furnace and sample orientation

Results & Discussion

Examples of the images obtained are shown in figure 2. Figure 2 (a) shows the original captured image, before image enhancement, for an Al-15wt%Cu sample run. The poor image contrast is found to be indicative of the entire experimental run. This discrepancy is attributed to the extremely high energy of the ID15 beamline. Even for the lowest energies, between 30 and 90 keV, the majority of the photons pass through the sample unabsorbed giving approximately 1.5 – 2% in total integrated absorption contrast between 200 μm of α-Al solid and Al-Cu liquids between 15-25wt%Cu. This puts the contrast close to the intrinsic noise level of the image acquisition system.

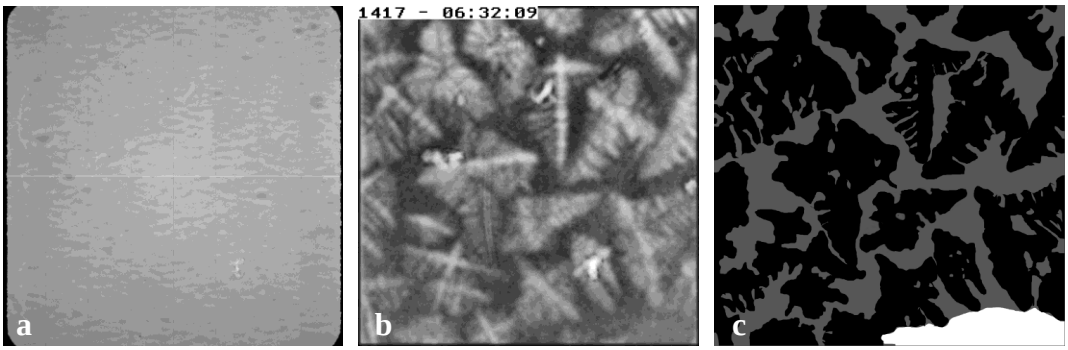

Figure 2. Al-15wt%Cu image acquisition data; (a) Original image; (b) Contrast enhanced image; (c) Envelope and Grain masking

Figure 2 (b) shows (a) post image enhancement through, flat fielding, noise cancellation, adaptive histogram adjustment and spatial convolution filtering. The spatial filtering method used was designed and implemented specifically for these images. While noise is still evident,

grains structures are clearly visible. Figure 2 (c) shows the process of envelope definition and solid α-Al extraction, with solid aluminum in black, coherency envelope in grey and outside envelope as white. In the case of rheological and thermal analysis [6], the point of coherency is determined at a discrete time based on changes in measured parameters, i.e. torque and temperature. In reality however, grain coherency is a transient process strongly governed by local undercoolings, solutal constitution and gravity-induced thermosolutal convection. Therefore degrees of coherency are occurring in any non-isothermal melt throughout the solidification process with no absolute time. It is also understood that once impingement occurs, primary growth ceases and dendritic coarsening dominates. With real time in-situ image acquisition it is possible to observe grain growth after nucleation, grain motion and finally impingement at the point of coherency. It is observed from these captured sequences that once individual grains become coherent, no further growth, either coarsening or preferential, occurs while grains are passing through the FOV. It is certain that post transport through the FOV, predictable solidification processes occur, however whilst visible, grains appear frozen in time at the point of coherency. It is proposed, therefore, to define a coherency envelope from which coherency fraction solid (f_{coh}) will be determined, based on the ratio of internal envelope solid area, V_S, to internal envelope total area, V_{EV}, equation (1).

$$f_{coh} = V_S / V_{EV} \tag{1}$$

Figure 3 illustrates the coherency concept. Isolated nucleated grains grow and eventually impinge, creating coherent network clusters, as was apparent in this study. In cases where solid growth encompasses the entire FOV, as in figure 2(b), the FOV will serve as the envelope boundary.

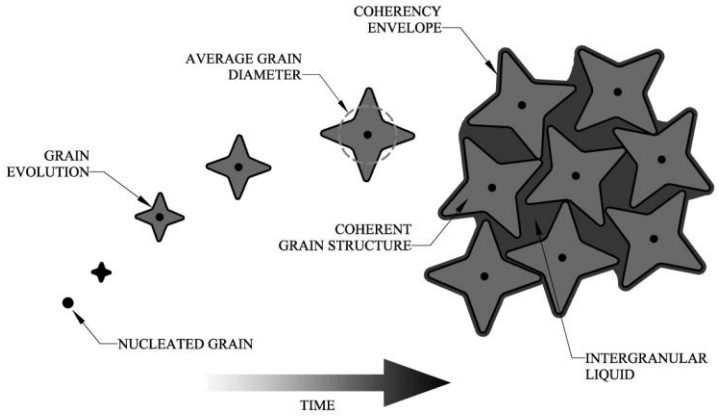

Figure 3. Coherency envelope definition

Due to the quasi-2D nature of the sample certain factors must be taken into consideration in the analysis. For instance, calculated solid fractions are based on area ratios, rather than volume ratios. This introduced unavoidable error into measurements as grains were observed to have varying thicknesses, less than or equal to the sample thickness. This was evidenced by instances of grain superposition observed during solidification. This error can be minimized in some respects by virtue of the ability to track grains from nucleation to impingement, continuously monitoring individual grain evolution. Also grains were observed to impinge mechanically on the crucible walls, i.e. get trapped between quartz slides, possibly distorting coherency events. Measurement reproducibility error was also evident due to manual definition of grain envelopes. To quantify this error a number of grain measurements were repeated several times to determine

average variation. This was calculated to be approximately 2.5%. Qualitatively, however, using consistent analytical methods the data showed minimal variation. Figure 4 shows a graph of the cooling rate across all samples versus coherency fraction solid. Cooling rate, in the case of a Bridgman furnace, is calculated as the product of thermal gradient and translation velocity. It is apparent from the data that change in cooling rate has no significant effect on f_{coh}, which supports the most recent published rheological/thermal comparisons [10]. Al-15wt%Cu samples were solidified initially at a low cooling rate, increasing step wise and then gradually increased to higher cooling rates. Al-25wt%Cu samples were solidified initially at low cooling rates and gradually decreased. Statistical correlation (r) was performed in the cooling rate/f_{coh} data and low values (<0.5) were observed for both alloy types suggesting a low degree of linearity between both variables. The coefficient of determination (r^2) for both samples was calculated at approximately 20% again supporting negative interdependence.

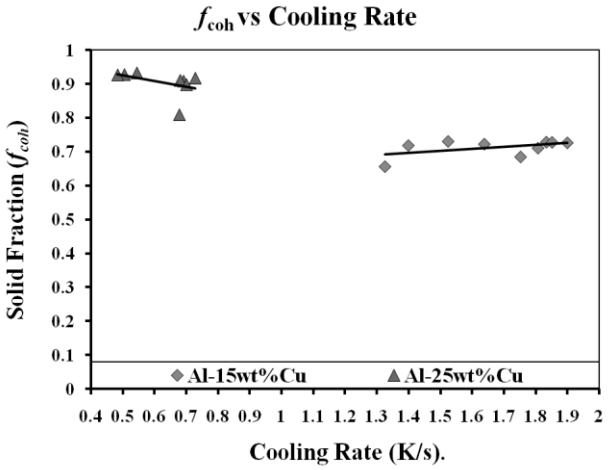

Figure 4. Cooling rate versus coherency fraction solid

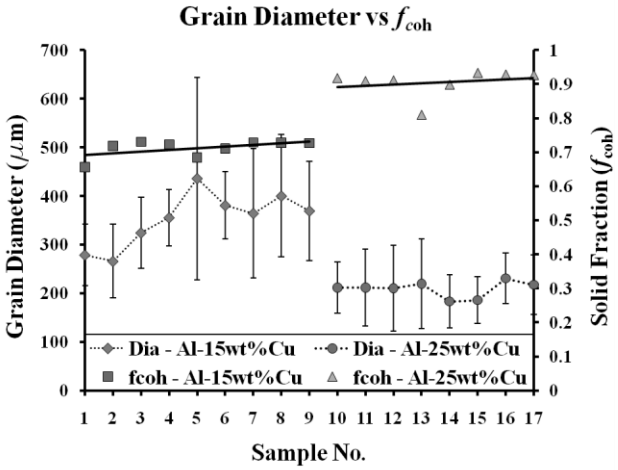

Figure 5. Grain diameter versus coherency fraction solid

Figure 5 shows the relationship between grain size and coherency fraction solid. Larger, and thus more dendritic, grains exhibit lower coherency fraction solid than the smaller cellular-equiaxed structures. This, again, supports previous experimental data as it is suggested smaller more numerous grains, exhibit slower growth thus impingement is delayed, increasing f_{coh}. It is also evident from figure 5 that there is significant deviation in grain size measured in individual coherency envelopes. Solidification sequences show grain nucleation at various locations and times ahead of the coherent network. It has already been suggested that movement of growing solid through the melt changes the local undercooling and composition, affecting subsequent growth. Evidence has also been presented of effects of so called solutal poisoning [19] caused by sedimenting solute ejected from growing grains. The combination of these solidification effects appears to be the cause of the observed grain size deviation. Finally figure 6 shows the so called fullness parameter, f_S, in relation to f_{coh}. It is not expected that this value should show any significant difference in trend however, it is expected to be higher than f_{coh}, as observed. The fullness, equation (2), parameter itself appears to be an appropriate measure of grain morphology, with large highly dendritic grains showing lower fullness and small globular grains exhibiting a large value of fullness.

$$f_S = V_{GS} / V_{GE} \qquad (2)$$

Figure 7 shows an example of the differences observed in morphological evolution. In figure 7 (a), a more elongated dendritic growth morphology is observed, with well defined secondary dendrite arm spacings. Figure 7 (b) shows, on average, a more circular and smaller grain size exhibiting the so called equiaxed-cellular morphology. Apparent from figure 7 is the higher granular solid fraction in (b), which stems from smaller grains allowing for more efficient coherent packing ultimately increasing the coherency fraction solid.

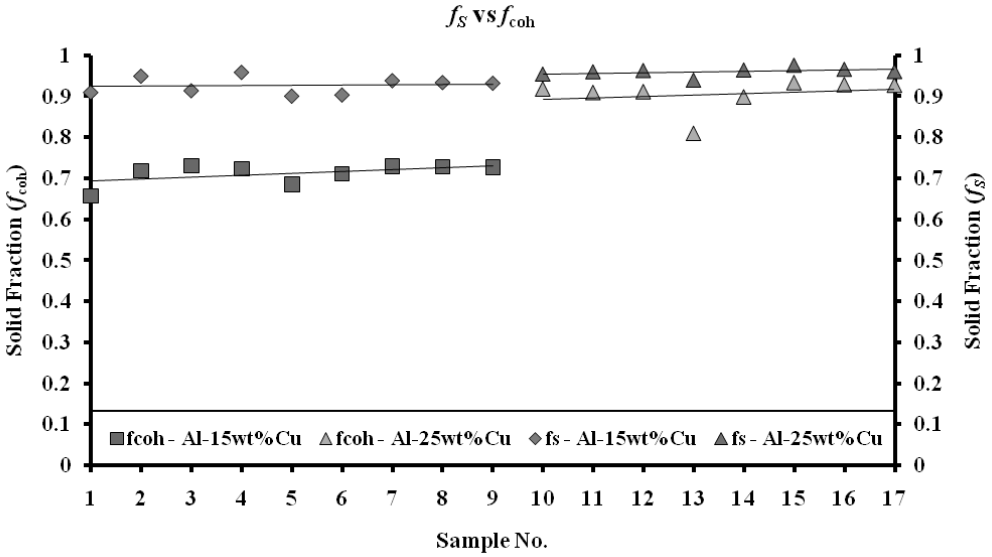

Figure 6. Fullness versus coherency fraction solid

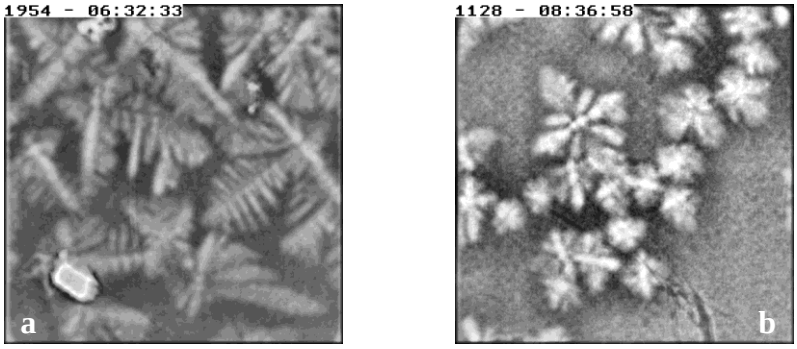

Figure 7. Al-15wt%Cu (a) and Al-25wt%Cu (b) morphological comparison

A first order approximation method of calculating the volume coherency fraction solid is proposed. Assuming the 2D solid fraction can be modeled as a spherical volume of solid proportional to the solid area and 2D coherency envelope can be modeled as a cubic volume element proportional to envelope area, the conversion is derived as follows:

$$V_S = \frac{4}{3\sqrt{\pi}} (A_S)^{3/2} \tag{3}$$

where V_S is the equivalent spherical solid volume based on the total captured solid area, A_S. Similarly V_{EV}, the cubic equivalent coherency envelope is determined using equation (4).

$$V_{EV} = (A_{EV})^{3/2} \tag{4}$$

where A_{EV} is the total area of the defined coherency envelope. The 3D coherency fraction, $f_{coh}\,3D$, is thus defined as the ratio of V_S to V_{EV} as expressed in equation (5).

$$f_{coh}\,3D = V_S \Big/ V_{EV} \tag{5}$$

Figure 8 shows the newly calculated volume coherency fraction solid for the captured data. As expected these values are consistently lower than the values calculated for equivalent areas however, they are still higher than published data. It should be noted, however, in-situ studies show direct observation of solidification phenomena in real time and there have been significant inconsistencies between rheological and thermal data suggesting deviation may be systematic.

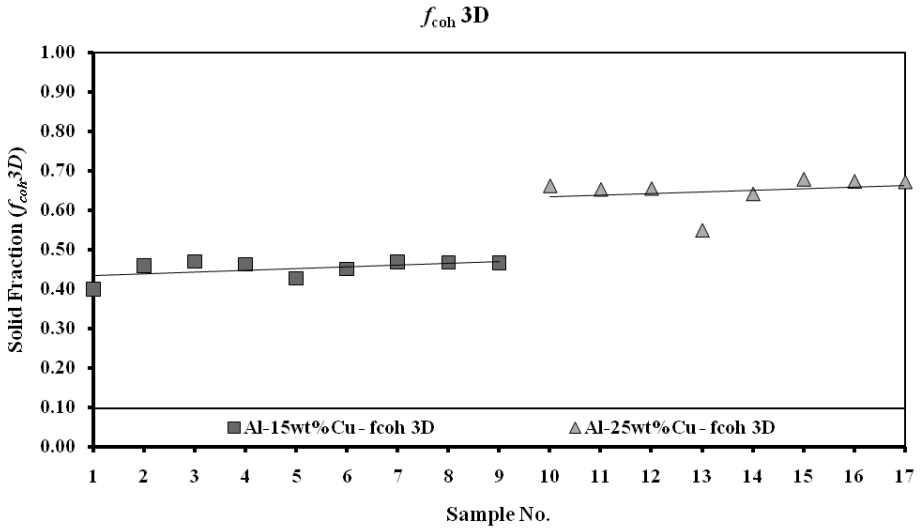

Figure 8. Volume based coherency fraction solid

Conclusions & Future Work

This document presents a preliminary study into the determination of fraction solid at the point of coherency. Qualitative agreement was found between this work and the work of Veldman *et al*. [10] in relation to cooling rate independence and increasing coherency fraction solid with decreasing grain size. It is observed here however, that decreasing grain size follows an increase in solute concentration which contradicts previous work. Previous solute concentrations analyzed however have been limited to low concentration and industrial compositions [6, 8], which may account for the discrepancy. Based on this study, further work is a required with alloy composition more consistent with previous rheological and thermal experimental campaigns in order to make quantitative comparisons. Correlations between coherency fraction solid and other grain attributes, i.e. aspect ratio, grain rotation and grain motion, are proposed for future investigation. The 2D to 3D conversion described here also requires further investigation and definition. The nature of the thin sample has the effect of distorting grain growth, as growth in the plane of the beam is suppressed while grain cross-sections become artificially enlarged. 2D to 3D conversions can therefore result in cumulative errors in predicting volumetric solid fractions. Microgravity experiments are also warranted to determine the significance of thermosolutal convection and buoyancy on coherency fraction solid.

Acknowledgements

The authors wish to acknowledge the financial support of the European Space Agency (ESA) under the PRODEX program, (Contract No. 90392). This work is part of the ESA-MAP (Microgravity Applications Promotion) project XRMON. Also the authors wish to thank Dr. Marco Di Michiel (Exp. Division, ESRF) for his assistance with the experiment, Dr. Shaun McFadden (now at Dublin Institute of Technology, Ireland) and Dr. Paul Schaffer (now at Hydro Aluminium, Norway) for their efforts in capturing the experimental data.

References

1. S. A. Metz and M. C. Flemings, *AFS Trans.*, (78) (1970), 453.
2. J. Claxton, *J. Metal.*, (1975), 14.
3. D. B. Spencer, R. Mehrabian, and M. C. Flemings, *Metallurgical Transactions*, 3 (1972), 1925-1932.
4. D. Brabazon, D. J. Browne, and A. J. Carr, *Materials Science and Engineering: A*, 356 (1-2) (2003), 69-80.
5. L. Backerud and B. Chalmers, *Trans Met Soc AIME*, 245 (2) (1969), 309-318.
6. G. Chai et al., *Metallurgical and Materials Transactions A*, 26 (1995), 965-970.
7. J. Tamminen, *Chem. Comm., Stockholm*, 2 (1988), 8-33.
8. L. Arnberg, G. Chai, and L. Backerud, *Materials Science and Engineering: A*, 173 (1-2) (1993), 101-103.
9. A. K. Dahle and L. Arnberg, *Materials Science and Engineering: A*, 225 (1-2) (1997), 38-46.
10. N. L. M. Veldman et al., *Metallurgical and Materials Transactions A*, 32 (2001), 147-155.
11. I. Dustin and W. Kurz, *Z. Metallkd*, 77 (1986), 265-73.
12. M. Rappaz and P. H. Thevoz, *Acta Metallurgica*, 35 (12) (1987), 2929-2933.
13. R. H. Mathiesen et al., *Physical Review Letters*, 83 (24) (1999), 5062.
14. H. N. Thi et al., *Journal of Physics D: Applied Physics*, 36 (10A) (2003), A83-A86.
15. H. Yasuda et al., *Journal of Crystal Growth*, 262 (1-4) (2004), 645-652.
16. R. H. Mathiesen et al., *Metallurgical and Materials Transactions B*, 33 (4) (2002), 613-623.
17. R. H. Mathiesen and L. Arnberg, *Materials Science and Engineering: A*, 413-414 (2005), 283-287.
18. R. H. Mathiesen and L. Arnberg, *Acta Materialia*, 53 (4) (2005), 947-956.
19. A. Bogno et al., *Transactions of the Indian Institute of Metals*, 62 (4-5) (2009), 427-431.